

THz Higher-Order Topological Photonics in Ge-on-Si Heterostructures

Ian Colombo¹, Pietro Minazzi¹, Emiliano Bonera¹, Fabio Pezzoli^{1*} and Jacopo Pedrini¹

¹ Dipartimento di Scienza dei Materiali, Università degli Studi di Milano-Bicocca and BiQuTe, via R. Cozzi 55, 20125 Milan (Italy)

* fabio.pezzoli@unimib.it

Abstract

We design germanium-based higher-order topological cavities for terahertz applications by breaking the symmetry of a two-dimensional photonic crystal following the Su-Schrieffer-Heeger model. Calculations demonstrate the parity inversion of the electric field in differently deformed unit cells. The interface between domains of opposite topology presents edge and corner modes. The former are chiral, locking light propagation to its helicity. The latter prove that Ge-based structures can be used as high-order topological photonic crystals. These findings can accelerate the development of Si-photonics components working in a spectral range of high technological interest.

Copyright attribution to authors.

This work is a submission to SciPost Physics.

License information to appear upon publication.

Publication information to appear upon publication.

Received Date

Accepted Date

Published Date

1

2 Contents

3	1 Introduction	1
4	2 Results and discussion	2
5	3 Conclusions	8
6	A Role of the {111} facets	8
7	B Details on the computational method	8
8	C Bandstructure of the PC as a function of d	11
9	References	11

10

11

12 1 Introduction

13 The comprehension and exploitation of the topological properties of matter led to the emer-
14 gence of research on topological insulators [1] and their photonic analogs, known as topo-

15 logical photonic crystals (TPC). [2, 3] TPCs have been shown to be promising for the fabrica-
16 tion of photonic integrated circuits thanks to exceptional features, e.g., directional and chiral
17 light propagation, [4–6] strong resistance to sharp bends, [7] and mathematical protection
18 from defect-induced scattering. [8] These properties are indeed expected to facilitate the im-
19 plementation of advanced photonic components such as directional, polarization-dependent
20 waveguides, [9–11] resonators, [12] drop-filters [13] and topological lasers. [7, 14, 15]

21 Lately, higher-order topology has been gaining attention in photonics research. In con-
22 trast to conventional topological insulators, higher-order topological insulators (HOTI) present
23 conductive states that are more than one dimension lower than the insulating state. [16, 17]
24 This has led to the concept of special two-dimensional (2D) TPCs, which can feature unusual
25 zero-dimensional (0D) corner states in addition to the conductive one-dimensional (1D) hinge
26 modes. The potential to exploit HOTIs to fully confine the electromagnetic field at a 0D cor-
27 ner and topologically protect it from undesired losses is fundamentally intriguing and strongly
28 appealing for applications, particularly because it might drastically boost lasing emission and
29 improve spectral purity. [14]

30 Although crystals with a trivial photonic band structure have already found applications in
31 the terahertz (THz), [18, 19] the extension of HOTIs into such frequency range has been very
32 limited thus far. The interest in this spectral regime comes from the inherent capacity to stream
33 high-frequency wide-bandwidth data; [20] a characteristic that offers significant prospects for
34 the advancement of wireless communication networks beyond existing 5G standards. [21, 22]
35 In addition to telecommunications, THz waves can have far-reaching consequences in various
36 fields, including quantum information, [21–23] non-destructive imaging, [24, 25] biological
37 sensing and diagnostics, [26, 27] security and defense. [28, 29] The development of efficient
38 THz photonic components and devices is thus a compelling task where TPC and HOTIs can
39 provide a leap forward with novel and yet untapped capabilities.

40 Another crucial factor in achieving this ambitious goal is the choice of materials platform
41 that can favor an industrial takeover while being, at the same time, suitable for the THz regime.
42 Germanium stands out as a solution to these two problems since it offers a transparency win-
43 dow that is spectrally broad, [30, 31] while being already present in microelectronic and pho-
44 tonic foundries. Ge-based high-quality photonic crystals (PC) can be indeed created using
45 conventional lithography and vertical etching of thin Ge-on-Si films [32–34] or by exploiting
46 self-assembly of Ge crystals directly on top of patterned Si substrates. [35] This can result in
47 high-volume production and opens the route toward monolithic integration of THz photonic
48 components into Si chips.

49 So far, literature reports have shown that Ge-on-Si heterostructures host promising, albeit
50 non-topological, photonic properties in the near-infrared region of the electromagnetic spec-
51 trum. [36–38] To unfold the Ge potential in exhibiting HOTI states in the THz regime, we
52 employ the finite elements method (FEM) to investigate photonic and topological properties
53 including the emerge of a photonic band gap (PBG) and the topology-induced spatial confine-
54 ment and directional propagation of light. In this work, we will concentrate on the model
55 system offered by the self-assembly of micron-sized Ge-on-Si rods. Their typical in-plane ar-
56 rangement can seemingly mimic 2D TPCs with a square geometry [14, 39–43] and their distinct
57 optical properties [44–48] can possibly expedite the practical realization of future, integrated
58 HOTI devices.

59 2 Results and discussion

60 Figure 1a shows the layout of a typical microstructure consisting of Ge-on-Si microcrystals. To
61 determine the photonic bandstructure of the 2D lattice as close as possible to the experimental

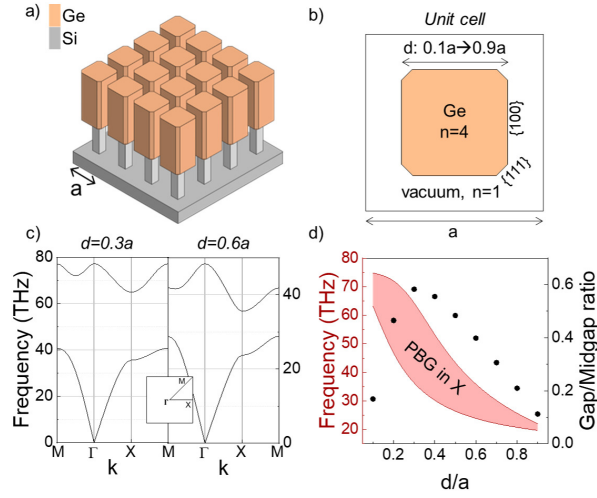


Figure 1: a) Sketch of the model photonic crystal (PC) based on a Ge (orange) on Si (grey) heterostructure (not to scale). [37] The lattice parameter is a . b) Scheme of the simulated unit cell of the PC. c) Simulated bandstructure of the PC calculated using finite element method for a Ge crystal size $d = 0.3a$ (left) and $d = 0.6a$ (right). Inset: Irreducible Brillouin Zone of the square lattice with high symmetry points indicated. d) Size of the photonic bandgap (PBG) calculated in the X point of the bandstructure (red shaded area) and gap/midgap ratio (black dots) as a function of d .

ones, [37] we simulated a unit cell composed of a pseudo-octagonal Ge microcrystal, featuring both $\{100\}$ and $\{111\}$ facets surrounded by vacuum. The $\{111\}$ facets are sub-wavelength and their role on determining the photonic bandstructure of the crystal is negligible, as shown in Figure 5 in Appendix A. The lattice parameter is $a = 2 \mu\text{m}$ to ensure experimental feasibility with conventional fabrication processes. [37] The size d of the Ge microcrystal was varied in the FEM calculations between $0.1a$ and $0.9a$. The refractive index of Ge has been extracted from the literature [49] and is $n \sim 4$, corresponding to the value measured in the THz region of the electromagnetic spectrum, where the extinction coefficient is zero and n itself can be considered constant for the purposes of the calculations. The geometry of the unit cell, together with the structure parameters, is reported in Figure 1b.

We performed a FEM simulation of the system eigenfrequencies with Comsol Multiphysics [50], using Floquet periodicity and varying the size d of the microcrystal to gather information on the optimal geometric parameters of the PC. The simulation was performed for the out-of-plane electric field configuration, also known as transverse magnetic (TM) modes. Further details on the simulation methods are reported in Appendix B. The simulation sweeps the wavevector \mathbf{k} along high symmetry directions in the irreducible Brillouin Zone (IBZ), yielding the photonic bandstructure that is reported in Figure 1c for two values of d , namely $d = 0.3a$ and $d = 0.6a$, corresponding to a microcrystal lateral size of 600 nm and 1200 nm, respectively. The calculated bandstructures for every value of d are reported in Figure 9 in Appendix C. The bandstructures present a large PBG in the THz region of the electromagnetic spectrum.

The bandstructures have similar shapes for different values of d , but its increase shifts the energy bands toward lower frequencies and apparently shrinks the amplitude of the PBG as shown in Figure 1d, which reports the size of the PBG at the X high-symmetry point of the IBZ as a function of d . The size of the gap increases with d and then decreases until it is almost negligible. This behavior is expected in 2D PCs dominated by a high refractive index material. [51] To compare the size of the PBG between the different structures, we normalized

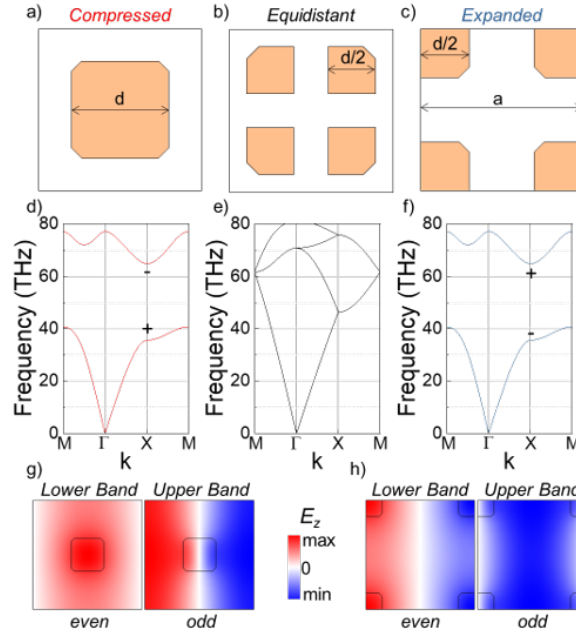


Figure 2: Scheme of the unit cell, simulated photonic bandstructure, and electromagnetic field distribution for the compressed (a,d,g), equidistant (b,e) and expanded (c,f,h) PCs when the lateral size of the Ge crystal d equals 0.3 times the lattice parameter a . The out-of-plane component of the electromagnetic field (TM mode) is computed at the X point of the IBZ. The parity of the wavefunction acts as a pseudospin, and the symmetry inversion (indicated by the $+$ and $-$) between the compressed and the expanded crystals is the fingerprint of a topological phase transition.

88 the bandgap to the midgap frequency. This renormalization method allows us to compare the
 89 relative amplitude of the PBG in structures with different geometries. [51] The calculation of
 90 the gap/midgap ratio in our case yields that the structure with the largest bandgap is that with
 91 $d = 0.3a$. Unless otherwise noted, hereafter we refer to this specific value of d .

92 It should be noted that the photonic properties of the simulated system depend on the spe-
 93 cific value of the lattice parameter a . However, the scaling invariance allows one to rigidly shift
 94 the energy of the PBG towards lower (higher) frequencies just by fabricating larger (smaller)
 95 unit cells. This powerful property provides great flexibility because it allows structures with a
 96 PBG in resonance with a desired frequency, e.g., the emission frequency of a quantum cascade
 97 structure. There are reports in the literature [52, 53] showing Ge/SiGe MQWs with interband
 98 emission at ~ 30 THz, a value that can already be reached with the PC described in Figure 1,
 99 e.g. for $d = 0.8a$. The structure can be further optimized by setting $d = 0.3a$, where the PBG
 100 is the largest, and increasing the lattice parameter a by a factor ~ 2 .

101 The 2D lattice composed of the semiconductor microcrystals can be seen as the periodic
 102 repetition of two different unit cells. The two structures can be considered the extreme case
 103 of a photonic extension of a 2D Su-Schrieffer-Heeger (SSH) lattice, [40, 54, 55] where a unit
 104 cell composed of four elements equidistant from both the center and the vertex of the cell is
 105 distorted, as shown in Figure 2. The first unit cell has a microcrystal with lateral size d at
 106 the center of the cell, as shown in Figure 1b or Figure 2a, and will from now on be referred
 107 to as *compressed*. The other structure consists of four quarters of a microcrystal with a width
 108 $\frac{d}{2}$ placed at the corners of the cell, as shown in Figure 2c. We will refer to this structure as
 109 *expanded*. The *equidistant* unit cell structure is reported in Figure 2b.

110 The bandstructures of the described lattices are reported in Figure 2d-f. The one of the *equidis-*

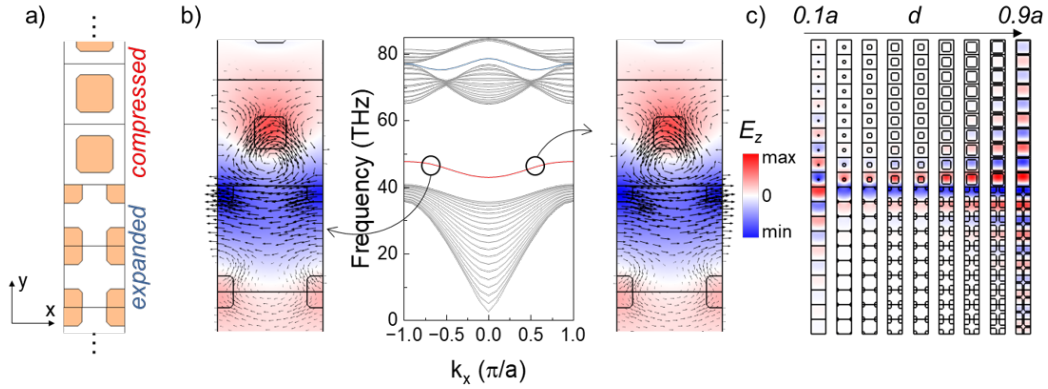


Figure 3: a) Schematics of a supercell consisting of a line interface between a compressed and expanded PCs. b) Calculated bandstructure of the supercell along the x direction. The bandstructure presents bulk bands (grey) with two sizeable gaps in which localized modes are present (red and blue curves). The modes are confined at the interface of the two regions of the PCs. The arrows overlaid on the electromagnetic field distribution underline the directionality of the propagation. c) Spatial distribution of the out-of-plane component of the electromagnetic field (E_z) in the supercell as a function of the lateral size of Ge d . The supercells are stacked horizontally as d increases from $0.1a$ to $0.9a$, where a is the lattice parameter.

111 tant PC (reported in Figure 2e) is gapless and shows a pseudo-Dirac point at the M and X high-
 112 symmetry points. The deformation of the unit cell opens a gap, as expected in the SSH model,
 113 and yields two identical photonic bandstructures for the *compressed* and *expanded* PCs. It is
 114 important to highlight that in a SSH model the band dispersion does not change with the in-
 115 version of the intra- and inter-cellular distances between the elements composing the unit cell,
 116 but the symmetry of the eigenfunctions is different, as they possess opposite parity. [40, 55]
 117 The topological invariant in SSH-like 2D photonic crystals like those described in this work
 118 can be classified by the Zak phase [40, 56], which is basically the integral of the Berry connec-
 119 tion on the Brillouin Zone. In some works [40] the bulk polarization \mathbf{P} is discussed instead
 120 of the Zak phase ϕ_Z , but the two are simply related by $\phi_Z = 2\pi\mathbf{P}$. The values of the Zak
 121 phase form a \mathbb{Z}_2 index in C_4 -symmetric topological crystals such as the one described in our
 122 work and can only take the values 0 or π for each direction for trivial or non-trivial topolo-
 123 gies, respectively. [41, 57] It is known from the literature [40, 41] that in structures akin to
 124 those described in this work, the Zak phase for the directions (x, y) is $(0, 0)$ for the *compressed*
 125 structure and (π, π) for the *expanded* structure, meaning that the structures are topologically
 126 trivial and nontrivial, respectively. To gather further insights on the bandstructure of the *ex-*
 127 *expanded* and *compressed* PCs, we calculated the out-of-plane electric field distribution E_z (TM
 128 mode) for such unit cells. Particularly, we investigate the E_z distribution at the X point of the
 129 bandstructure, where the PBG opens up. The E_z distribution maps are reported in Figure 2g,i.
 130 Here, the *compressed* PC presents an even E_z distribution in the lower band and an odd dis-
 131 tribution in the high-energy band. The opposite occurs in the *expanded* structure. This parity
 132 inversion confirms the equivalence of the two PC structures to a 2D SSH model. Therefore,
 133 the *compressed* and *expanded* PC belongs to distinct topological phases, where the parity of the
 134 bands can be considered as the topological invariant. In particular, the *compressed* structure is
 135 an ordinary insulator, while the *expanded* is topologically nontrivial.

136 One of the fingerprints of a topological transition is the so-called bulk, edge correspon-
 137 dence, that is the emergence of spatially confined guided modes at the boundary between two
 138 domains with different band topology. [1, 5, 7, 58, 59] Figure 3a reports the schematic of an

139 interface between the two PCs characterized by distinct topological invariants. For its charac-
 140 terization we designed a so-called *supercell* composed of a ribbon of 20 unit cells where the top
 141 (bottom) 10 unit cells are *compressed* (*expanded*). In other words, the top half of the supercell
 142 is an ordinary insulator, while the bottom half is topologically nontrivial. The FEM simulation
 143 of this structure is performed with periodic conditions along the x direction, and the eigenfre-
 144 quencies are calculated as a function of k_x , from $-\frac{\pi}{a}$ to $\frac{\pi}{a}$. A perfectly matched layer is used
 145 as the boundary condition for the top and bottom of the ribbon to simulate an infinite PC.
 146 The resulting bandstructure is shown in Figure 3b. It presents a large number of bulk modes
 147 and two energy gaps, the larger of which covers the interval between 41 and 65 THz, while
 148 a second, non complete one is at around 75 THz. For the scope of this work, we focus on
 149 the full PBG at lower energy. The bandgap frequencies are the same as those calculated for
 150 the bulk unit cells along the $\Gamma-X$ direction (see Figure 2). The presence of a single mode in
 151 the PBG, located at ~ 45 THz, is a fingerprint of the interface of two phases with a different
 152 topological invariant. Such a mode is spatially localized at the interface of the two domains,
 153 as is shown by the plot of E_z (see Figure 3b), with the electric field mostly penetrating the
 154 high-index structure. The arrows overlaid on the E_z map are the local Poynting vectors that
 155 represents the direction of propagation of the electromagnetic wave. The representation of
 156 the Poynting vector allows us to underline the presence of unidirectional propagating modes,
 157 that can be selectively coupled through helical excitation. [3, 5, 60] Figure 3c shows that when
 158 d is varied the imbalance between the air and Ge fractions affects the confinement of the edge
 159 mode, so that the field is almost perfectly localized within the two interfacial unit cells only
 160 for d ranging from $0.2a$ to $0.5a$.

161 The demonstration of the presence of optical modes at the interface between domains
 162 suggests a possible application of Ge-on-Si photonic architectures as on-chip THz waveguides
 163 in topological circuits. We can further extend our results by designing a 2D device that could
 164 also exploit the generation of higher-order topological modes at the intersection between such
 165 hinge modes. Figure 4a introduces a resonator composed of a square of the *expanded* PC having
 166 a side of 9-unit cells, surrounded by a cladding frame consisting of 4-unit cells of the *compressed*
 167 PC defining an interface that supports the mode described in Figure 3. The solutions of the
 168 eigenvalue analysis for the resonator are separated in four well-defined frequency regions, as
 169 shown in Figure 4b,c. The nature of these modes can be determined by analyzing the electric
 170 field distribution, as shown in Figure 4d-g. The electromagnetic field maps for solutions for
 171 frequencies < 41 THz (see Figure 4d) and > 65 THz (see Figure 4g) clearly demonstrate
 172 the bulk nature of the modes, that permeate vast regions of the PC. In the frequency range
 173 pertaining to the PBG two well separated sets of solutions are present at ~ 47 THz and at **55**
 174 THz. First, we focus on the four degenerate modes at **55** THz that dominate the energy density
 175 spectrum reported in Figure 4c. The map of the electric field distribution, reported in Figure
 176 4f, shows that these are extremely localized 0D corner modes. Their existence demonstrates
 177 that the structure described in this work is a higher-order TPC characterized by a bulk-edge-
 178 corner correspondence. [61] Moreover, localized corner modes are extremely interesting for
 179 their strong confinement properties and can be exploited for their possible applications to
 180 devices that need high-quality factor resonators such as light emitters, sensors, and non-linear
 181 systems. [40, 41, 62, 63]

182 We now focus on the lower energy modes, found at frequency around **47** THz. The electro-
 183 magnetic field distribution shows that these are edge modes confined at the interface between
 184 the trivial and topological PC structures. Their study can give further insight on the topological
 185 properties of the PC and how they influence the propagation of light at the interface between
 186 the two topologically-distinct domains. As described above, a characteristic property of TPCs
 187 is the directional propagation of light, which is related to its degree of circular polarization. To
 188 demonstrate this feature, we simulated the propagation of circularly polarized light by using

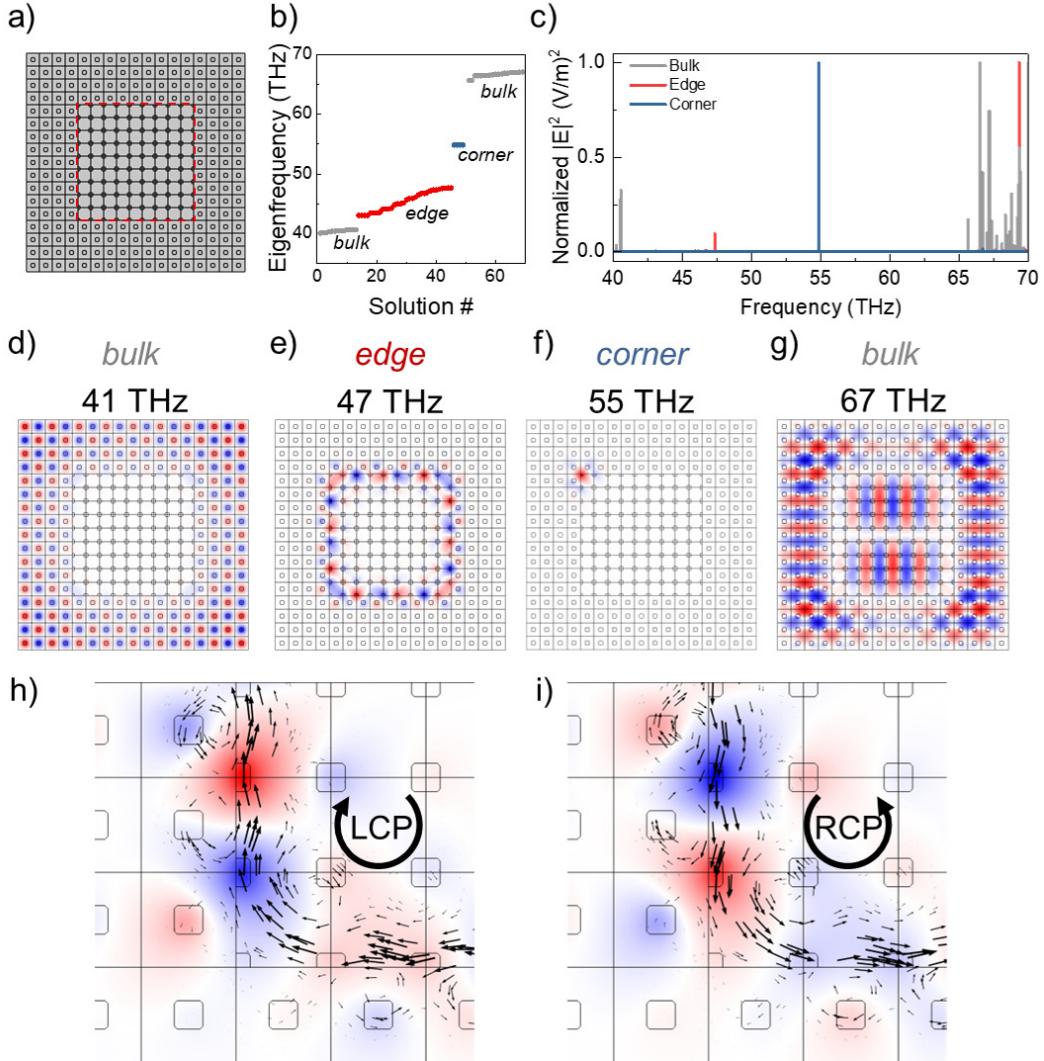


Figure 4: a) Schematics of a resonator composed of a square interface between an expanded PC surrounded by a compressed PC ($d = 0.3a$). The interface is marked with a red dashed line. b) Eigenfrequency values of the resonator as a function of the solution number. Four groups can be identified that correspond to bulk modes (low- and high-energy, grey), edge (red), and corner (blue) modes. c) Normalized field intensity as a function of the frequency, highlighting the bulk, edge and corner modes. d-g) Distribution of the out-of-plane component of the electric field at four significant frequencies corresponding to a low-energy bulk mode (d), edge mode (e), corner mode (f), and a high-energy bulk mode (g). h,i) Electromagnetic field E_z distribution at the bottom left corner of the resonator, when the resonator is excited with left (h) and right (i) circularly polarized light. The arrows at the interface between the topologically distinct regions are the Poynting vectors, highlighting a direct correspondence between light polarization and the direction of propagation.

189 an array of opportunely spaced phased dipoles localized at the interface between the topologi-
190 cally distinct regions. [64] The overlay of the Poynting vector on the electromagnetic field map,
191 shown in Figure 4h-i, demonstrates how the propagation is strongly directional and locked to
192 the degree of circular polarization, allowing chiral propagation at the interface of the PCs in
193 the THz range.

194 3 Conclusions

195 We demonstrated the possibility of achieving higher-order topological effects in the THz regime
196 in a PC composed of group IV heteroepitaxial microstructures. Such a HOTIs can be utilized
197 for the development of elemental components of photonic circuitries such as resonators and
198 waveguides. By combining Ge-based heterostructures with the intrinsic scalability of PCs one
199 can obtain devices working in a wide range of frequencies, possibly from mid-infrared to the
200 THz. Furthermore, the capacity to embed THz emitters in the microstructures in the form of
201 Ge/SiGe quantum wells might open a pathway to realize integrated, topological lasers with
202 a small footprint and high throughput that operate within technologically relevant spectral
203 regions.

204 Acknowledgements

205 The authors thank A. Marzegalli for technical assistance and L. Miglio for fruitful discussions.

206 **Funding information** This work has been funded by the European Union’s Horizon Europe
207 Research and Innovation Programme under agreement 101070700. Support from PNRR MUR
208 project PE0000023-NQSTI is also acknowledged. J.P acknowledges financial support from
209 FSE REACT-EU (grant 2021-RTDAPON-144).

210 A Role of the {111} facets

211 The role of the microcrystal faceting was investigated by comparing the photonic bandstructure
212 of the unit cell shown in Figure 1 to that of the same unit cell but with the Ge microcrystal only
213 possessing {100} facets, i.e. a perfect square. The bandstructures are almost identical, if not
214 for a negligible red-shift for the structure without {111} facets, most likely determined by the
215 slightly larger fraction of the unit cell that is occupied by the high refractive index material,
216 that is known to shift the energy gap towards lower energy. This analysis shows that the role
217 of the {111} facets is negligible, as expected by strongly sub-wavelength fine-structuring of
218 the elements composing the photonic crystal.

219 B Details on the computational method

220 The photonic simulations were performed with Comsol Multiphysics 6.1, by using the *wave op-*
221 *tics module*. The chosen physics was *electromagnetic wave, frequency domain* and we performed
222 an *eigenfrequency* analysis.

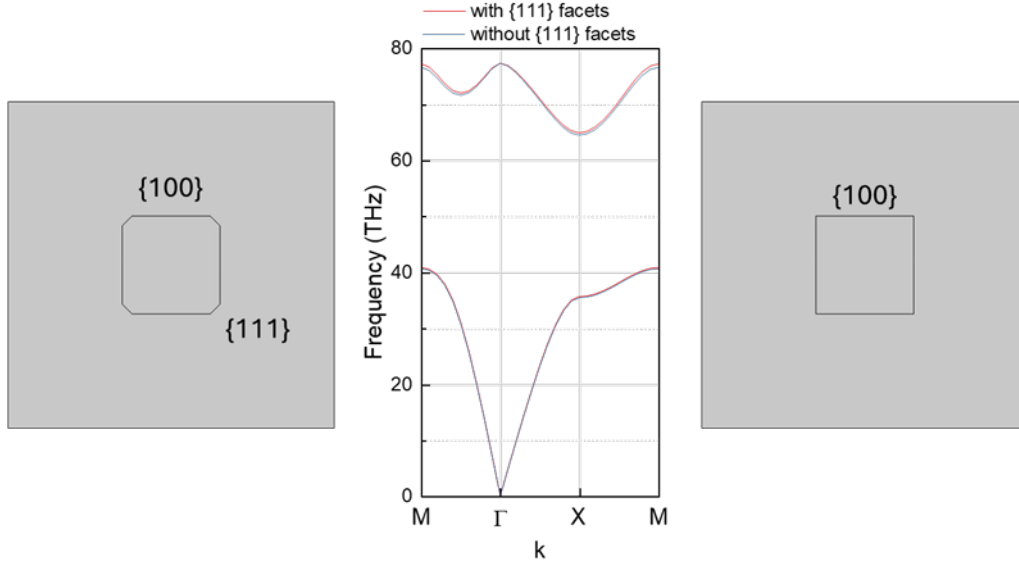


Figure 5: Photonic bandstructure for a *compressed* unit cell with the Ge element presenting both $\{100\}$ and $\{111\}$ facets (left) compared to one with only $\{100\}$ facets (right).

223 Eigenfrequency calculation for the unit cells

224 The solutions were calculated for the out-of-plane electromagnetic wave (TM mode) by using
 225 Floquet periodic boundary conditions both in the x and y direction. The wave vectors k_x and
 226 k_y were swept by mapping the high symmetry directions of the square irreducible Brillouin
 227 Zone (see the inset in Figure 1c) by with a parameter k , in such a way that the high symmetry
 228 points M, Γ , X, and M correspond to $k = 0$, $k = 1$, $k = 2$, $k = 3$, respectively. The parameter
 229 k was increased by 0.1 from 0 to 3 for a total of 32 simulated wavevector values (**See Figure**
 230 **S4**). For the supercell, the solutions were calculated for the out-of-plane electromagnetic wave
 231 (TM mode) by using Floquet periodic boundary conditions only in the x direction. The wave
 232 vector k_x was swept from $-\pi/a$ to π/a . The k_x parameter was increased by $0.1 \times \pi/a$. For
 233 the resonator, the solutions were calculated for the out-of-plane electromagnetic wave (TM
 234 mode) by using absorbing boundaries to simulate infinite propagation.

235 Mesh size

236 The simulations were performed with a free triangular mesh with the *finer* setting, correspond-
 237 ing to a mesh of triangular elements with maximum element size of 78 nm and a minimum
 238 element size of 0.25 nm. The parameters were chosen to have a good trade-off between com-
 239 putational speed and accuracy of the simulation. Nevertheless, by increasing or decreasing
 240 the mesh size to the *normal* or *extremely fine* values, the simulation yields the same results.
 241 The parameters for the meshes that were tested are reported in Table 1, while the meshed unit
 242 cells are shown in Figure 6 and the calculated bandstructures for each meshed cell are shown
 243 in Figure 7.

244 Error and convergence

245 A sample convergence plot for the calculation of the photonic bandstructure of the *compressed*
 246 unit cell, with the *finer* mesh described in Table 1 is reported in Figure 8. The plot shows the

	Normal	Finer	Extremely fine
Max. element size (nm)	134	74	20
Min. element size (nm)	0.60	0.25	0.04
Max. element growth rate	1.3	1.25	1.1
Curvature factor	0.3	0.25	0.2

Table 1: Parameters of three meshes tested for the computational work.

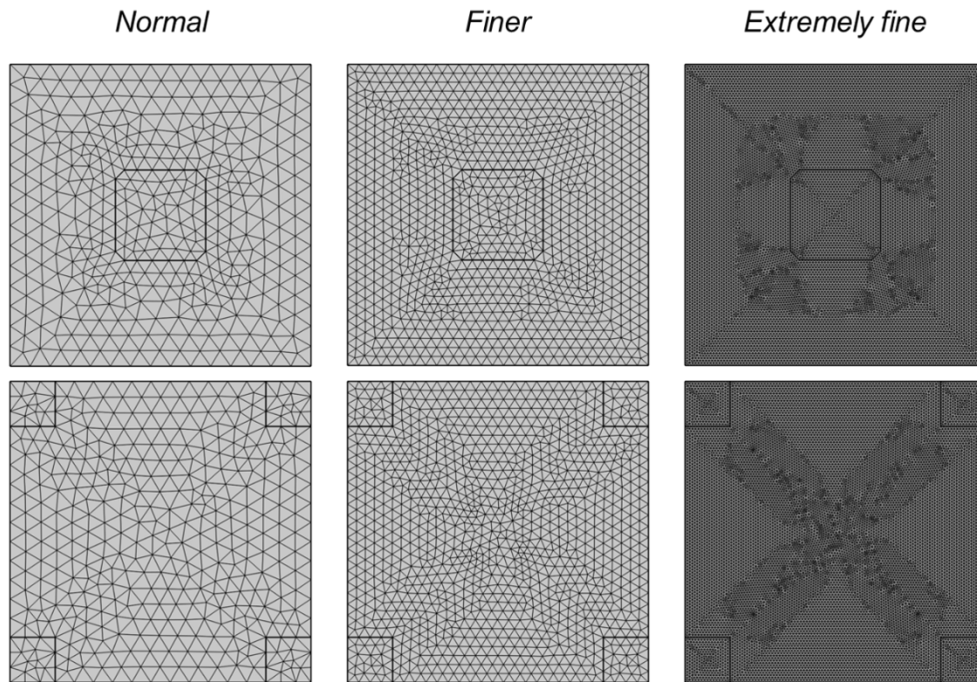


Figure 6: Meshed unit cells with the parameters described in Table 1.

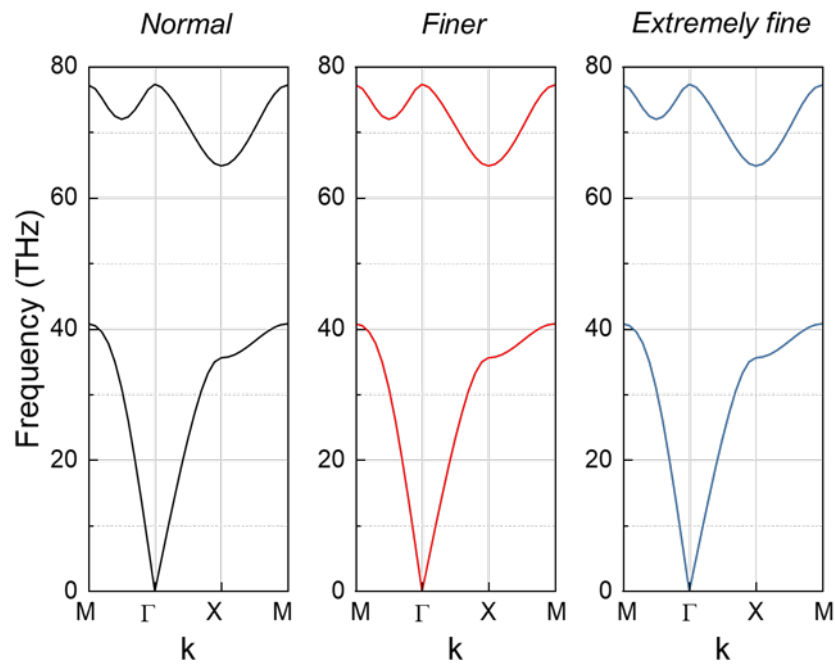


Figure 7: Photonic bandstructure calculated with the three meshes described in table S1.

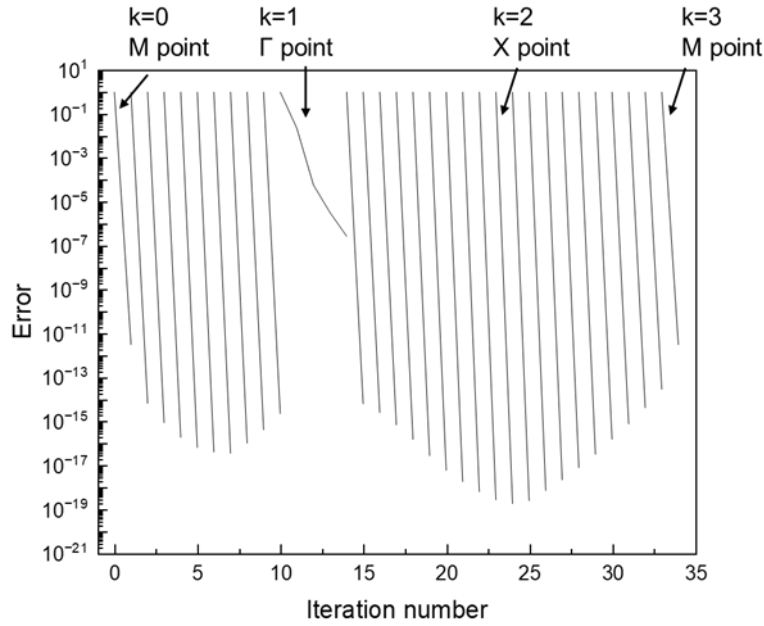


Figure 8: Convergence plot for the calculation of the bandstructure of the *compressed* unit cell, performed with *finer* mesh settings described in Table 1. Each line corresponds to a k value, and highlighted are the points of high symmetry of the IBZ.

247 number of iterations needed to reach convergence for each k point of the bandstructure. The
 248 calculation error is generally around or lower than 10^{-15} and is reached at the first iteration
 249 of the eigenfrequency calculation. This is not true for the Γ point of the bandstructure that,
 250 having an eigenfrequency close to zero, is less accurate and needs three iterations to reach an
 251 error of 10^{-7} . Nevertheless, it is important to note that in the X point of the bandstructure,
 252 i.e. where the topological inversion occurs, the error is of the order of 10^{-19} .

253 C Bandstructure of the PC as a function of d

254 The bandstructure of the *compressed* unit cell was investigated as a function of the microcrystal
 255 size d , from $d = 0.1a$ to $d = 0.9a$. The results of such investigation are reported in Figure 9.
 256 A full photonic bandgap is present only for $0.2a < d < 0.7a$. However, the photonic bandgap
 257 in X, point of the IBZ where the topological inversion occurs, is present for every value of d .
 258 The increase of the average refractive index of the unit cell, that is obviously proportional to
 259 the size of the microcrystal, shifts the photonic bandstructure towards lower frequencies, with
 260 a photonic bandgap in X centered at ~ 70 THz for $d = 0.1a$ and at ~ 21 THz for $d = 0.9a$.

261 References

- 262 [1] M. Z. Hasan and C. L. Kane, *Colloquium: Topological insulators*, *Reviews of Modern*
 263 *Physics* **82**(4), 3045 (2010), doi:[10.1103/RevModPhys.82.3045](https://doi.org/10.1103/RevModPhys.82.3045).
- 264 [2] L. Lu, J. D. Joannopoulos and M. Soljačić, *Topological photonics*, *Nature Photonics* **8**(11),
 265 821 (2014), doi:[10.1038/nphoton.2014.248](https://doi.org/10.1038/nphoton.2014.248), [1408.6730](https://doi.org/10.1038/nphoton.2014.248).

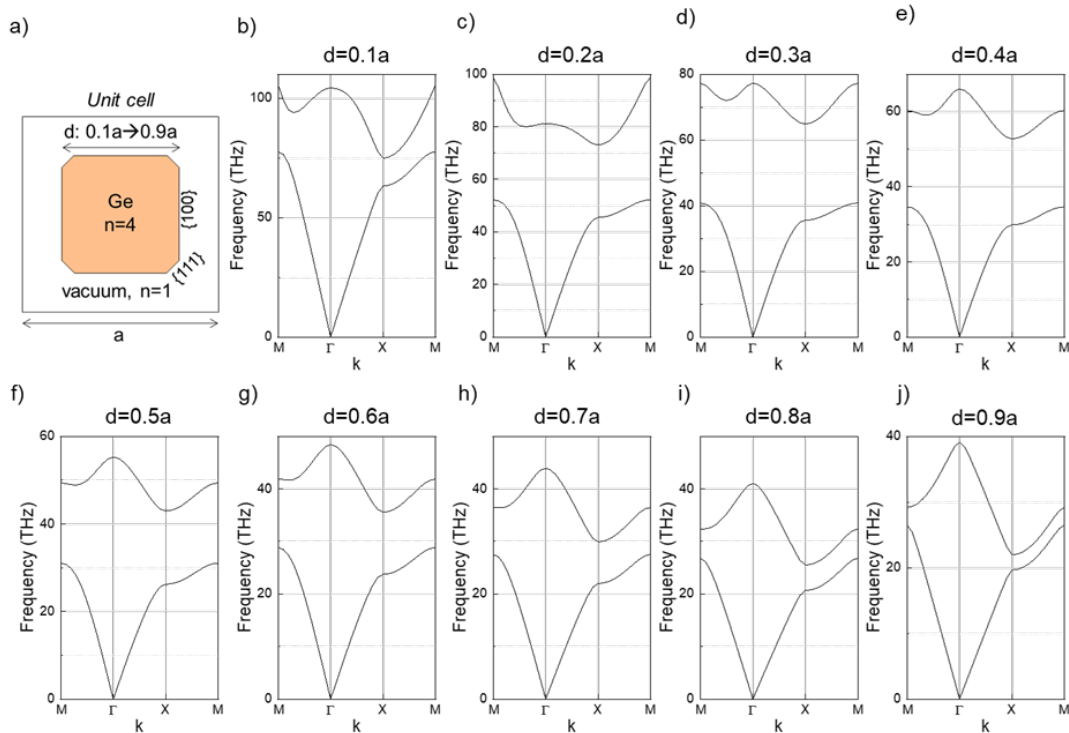


Figure 9: Photonic bandstructure calculated with the finite element method for the PC described in a) as a function of the ratio between the size of the Ge element d and the lattice parameter a .

- 266 [3] T. Ozawa, H. M. Price, A. Amo, N. Goldman, M. Hafezi, L. Lu, M. C. Rechtsman, D. Schuster,
 267 J. Simon, O. Zilberberg and I. Carusotto, *Topological photonics*, *Reviews of Modern*
 268 *Physics* **91**, 015006 (2019), doi:[10.1103/RevModPhys.91.015006](https://doi.org/10.1103/RevModPhys.91.015006).
- 269 [4] P. Lodahl, S. Mahmoodian, S. Stobbe, A. Rauschenbeutel, P. Schneeweiss, J. Volz,
 270 H. Pichler and P. Zoller, *Chiral quantum optics*, *Nature* **541**(7638), 473 (2017),
 271 doi:[10.1038/nature21037](https://doi.org/10.1038/nature21037), 1608.00446.
- 272 [5] L. H. Wu and X. Hu, *Scheme for achieving a topological photonic crystal by using dielectric material*,
 273 *Physical Review Letters* **114**(22), 1 (2015),
 274 doi:[10.1103/PhysRevLett.114.223901](https://doi.org/10.1103/PhysRevLett.114.223901).
- 275 [6] J. W. Dong, X. D. Chen, H. Zhu, Y. Wang and X. Zhang, *Valley photonic crystals for control*
 276 *of spin and topology*, *Nature Materials* **16**(3), 298 (2017), doi:[10.1038/nmat4807](https://doi.org/10.1038/nmat4807).
- 277 [7] Y. Zeng, U. Chattopadhyay, B. Zhu, B. Qiang, J. Li, Y. Jin, L. Li, A. G. Davies, E. H. Linfield,
 278 B. Zhang, Y. Chong and Q. J. Wang, *Electrically pumped topological laser with valley edge*
 279 *modes*, *Nature* **578**(7794), 246 (2020), doi:[10.1038/s41586-020-1981-x](https://doi.org/10.1038/s41586-020-1981-x).
- 280 [8] Z. Wang, Y. Chong, J. D. Joannopoulos and M. Soljačić, *Observation of unidirectional*
 281 *backscattering-immune topological electromagnetic states*, *Nature* **461**(7265), 772 (2009),
 282 doi:[10.1038/nature08293](https://doi.org/10.1038/nature08293).
- 283 [9] M. Jalali Mehrabad, A. P. Foster, R. Dost, E. Clarke, P. K. Patil, A. M. Fox, M. S. Skolnick
 284 and L. R. Wilson, *Chiral topological photonics with an embedded quantum emitter*, *Optica*
 285 **7**(12), 1690 (2020), doi:[10.1364/OPTICA.393035](https://doi.org/10.1364/OPTICA.393035).

- 286 [10] Y. Yang, Y. F. Xu, T. Xu, H.-X. Wang, J.-H. Jiang, X. Hu and Z. Hang, *Visual-*
287 *ization of a unidirectional electromagnetic waveguide using topological photonic crys-*
288 *tals made of dielectric materials*, Physical Review Letters **120**(21), 217401 (2018),
289 doi:[10.1103/PhysRevLett.120.217401](https://doi.org/10.1103/PhysRevLett.120.217401).
- 290 [11] N. Parappurath, F. Alpeggiani, L. Kuipers and E. Verhagen, *Direct observation of topolog-*
291 *ical edge states in silicon photonic crystals: Spin, dispersion, and chiral routing*, Science
292 Advances **6**(10), eaaw4137 (2020), doi:[10.1126/sciadv.aaw4137](https://doi.org/10.1126/sciadv.aaw4137).
- 293 [12] M. Jalali Mehrabad, A. P. Foster, R. Dost, E. Clarke, P. K. Patil, I. Farrer, J. Heffernan, M. S.
294 Skolnick and L. R. Wilson, *A semiconductor topological photonic ring resonator*, Applied
295 Physics Letters **116**(6), 061102 (2020), doi:[10.1063/1.5131846](https://doi.org/10.1063/1.5131846).
- 296 [13] M. J. Mehrabad, A. P. Foster, N. J. Martin, R. Dost, E. Clarke, P. K. Patil, M. S. Skolnick and
297 L. R. Wilson, *Chiral topological add-drop filter for integrated quantum photonic circuits*,
298 Optica **10**(3), 415 (2023), doi:[10.1364/OPTICA.481684](https://doi.org/10.1364/OPTICA.481684).
- 299 [14] C. Han, M. Kang and H. Jeon, *Lasing at Multidimensional Topological States in*
300 *a Two-Dimensional Photonic Crystal Structure*, ACS Photonics **7**(8), 2027 (2020),
301 doi:[10.1021/acsp Photonics.0c00357](https://doi.org/10.1021/acsp Photonics.0c00357).
- 302 [15] Y. Ota, R. Katsumi, K. Watanabe, S. Iwamoto and Y. Arakawa, *Topological photonic crystal*
303 *nanocavity laser*, Communications Physics **1**(1), 4 (2018), doi:[10.1038/s42005-018-](https://doi.org/10.1038/s42005-018-0083-7)
304 [0083-7](https://doi.org/10.1038/s42005-018-0083-7), [1806.09826](https://doi.org/10.1038/s42005-018-0083-7).
- 305 [16] F. Schindler, A. M. Cook, M. G. Vergniory, Z. Wang, S. S. P. Parkin, B. A. Bernevig and
306 T. Neupert, *Higher-order topological insulators*, Science Advances **4** (2018).
- 307 [17] A. Dutt, M. Minkov, I. A. Williamson and S. Fan, *Higher-order topological insulators in*
308 *synthetic dimensions*, Light: Science and Applications **9**(1) (2020), doi:[10.1038/s41377-](https://doi.org/10.1038/s41377-020-0334-8)
309 [020-0334-8](https://doi.org/10.1038/s41377-020-0334-8), [1911.11310](https://doi.org/10.1038/s41377-020-0334-8).
- 310 [18] W. Withayachumnankul, M. Fujita and T. Nagatsuma, *Integrated silicon photonic crystals*
311 *toward terahertz communications*, Advanced Optical Materials **6**(16), 1800401 (2018),
312 doi:[10.1002/adom.201800401](https://doi.org/10.1002/adom.201800401).
- 313 [19] R. A. S. D. Koala, M. Fujita and T. Nagatsuma, *Nanophotonics-inspired all-silicon wave-*
314 *guide platforms for terahertz integrated systems*, Nanophotonics **11**(9), 1741 (2022),
315 doi:[10.1515/nanoph-2021-0673](https://doi.org/10.1515/nanoph-2021-0673), Publisher: De Gruyter.
- 316 [20] T. Nagatsuma, G. Ducournau and C. C. Renaud, *Advances in terahertz com-*
317 *munications accelerated by photonics*, Nature Photonics **10**(6), 371 (2016),
318 doi:[10.1038/nphoton.2016.65](https://doi.org/10.1038/nphoton.2016.65).
- 319 [21] Y. Yang, Y. Yamagami, X. Yu, P. Pitchappa, J. Webber, B. Zhang, M. Fujita, T. Nagatsuma
320 and R. Singh, *Terahertz topological photonics for on-chip communication*, Nature Photon-
321 ics **14**(7), 446 (2020), doi:[10.1038/s41566-020-0618-9](https://doi.org/10.1038/s41566-020-0618-9), [1904.04213](https://doi.org/10.1038/s41566-020-0618-9).
- 322 [22] A. Kumar, M. Gupta, P. Pitchappa, N. Wang, M. Fujita and R. Singh, *Terahertz topological*
323 *photonic integrated circuits for 6G and beyond: A Perspective*, Journal of Applied Physics
324 **132**(14), 140901 (2022), doi:[10.1063/5.0099423](https://doi.org/10.1063/5.0099423).
- 325 [23] A. Leitenstorfer, A. S. Moskalenko, T. Kampfrath, J. Kono, E. Castro-Camus, K. Peng,
326 N. Qureshi, D. Turchinovich, K. Tanaka, A. G. Markelz, M. Havenith, C. Hough *et al.*, *The*
327 *2023 terahertz science and technology roadmap*, Journal of Physics D: Applied Physics
328 **56**(22), 223001 (2023), doi:[10.1088/1361-6463/acbe4c](https://doi.org/10.1088/1361-6463/acbe4c).

- 329 [24] K. Kawase, Y. Ogawa, Y. Watanabe and H. Inoue, *Non-destructive terahertz imag-*
330 *ing of illicit drugs using spectral fingerprints*, *Optics Express* **11**(20), 2549 (2003),
331 doi:[10.1364/oe.11.002549](https://doi.org/10.1364/oe.11.002549).
- 332 [25] C. Jansen, S. Wietzke, O. Peters, M. Scheller, N. Vieweg, M. Salhi, N. Krumbholz, C. Jör-
333 dens, T. Hochrein and M. Koch, *Terahertz imaging: Applications and perspectives*, *Applied*
334 *Optics* **49**(19) (2010), doi:[10.1364/AO.49.000E48](https://doi.org/10.1364/AO.49.000E48).
- 335 [26] P. H. Siegel, *Terahertz technology in biology and medicine*, *IEEE Trans-*
336 *actions on Microwave Theory and Techniques* **52**(10), 2438 (2004),
337 doi:[10.1109/TMTT.2004.835916](https://doi.org/10.1109/TMTT.2004.835916).
- 338 [27] X. Yang, X. Zhao, K. Yang, Y. Liu, Y. Liu, W. Fu and Y. Luo, *Biomedical Applications*
339 *of Terahertz Spectroscopy and Imaging*, *Trends in Biotechnology* **34**(10), 810 (2016),
340 doi:[10.1016/j.tibtech.2016.04.008](https://doi.org/10.1016/j.tibtech.2016.04.008).
- 341 [28] J. F. Federici, B. Schulkin, F. Huang, D. Gary, R. Barat, F. Oliveira and D. Zimdars, *THz*
342 *imaging and sensing for security applications - Explosives, weapons and drugs*, *Semicon-*
343 *ductor Science and Technology* **20**(7) (2005), doi:[10.1088/0268-1242/20/7/018](https://doi.org/10.1088/0268-1242/20/7/018).
- 344 [29] Y. C. Shen, T. Lo, P. F. Taday, B. E. Cole, W. R. Tribe and M. C. Kemp, *Detection and*
345 *identification of explosives using terahertz pulsed spectroscopic imaging*, *Applied Physics*
346 *Letters* **86**(24), 1 (2005), doi:[10.1063/1.1946192](https://doi.org/10.1063/1.1946192).
- 347 [30] D. Marris-Morini, V. Vakarin, J. M. Ramirez, Q. Liu, A. Ballabio, J. Frigerio, M. Mon-
348 tesinos, C. Alonso-Ramos, X. Le Roux, S. Serna, D. Benedikovic, D. Chrastina *et al.*,
349 *Germanium-based integrated photonics from near- to mid-infrared applications*, *Nanopho-*
350 *tonics* **7**(11), 1781 (2018), doi:[10.1515/nanoph-2018-0113](https://doi.org/10.1515/nanoph-2018-0113).
- 351 [31] M. Montesinos-Ballester, V. Vakarin, J. M. Ramirez, Q. Liu, C. Alonso-Ramos, X. Le Roux,
352 J. Frigerio, A. Ballabio, A. Barzaghi, L. Deniel, D. Bouville, L. Vivien *et al.*, *Optical mod-*
353 *ulation in Ge-rich SiGe waveguides in the mid-infrared wavelength range up to 11 μ m*,
354 *Communications Materials* **1**(1), 8 (2020), doi:[10.1038/s43246-019-0003-8](https://doi.org/10.1038/s43246-019-0003-8).
- 355 [32] M. El Kurdi, S. David, X. Checoury, G. Fishman, P. Boucaud, O. Kermarrec, D. Bensahel
356 and B. Ghyselen, *Two-dimensional photonic crystals with pure germanium-on-insulator*,
357 *Optics Communications* **281**(4), 846 (2008), doi:[10.1016/j.optcom.2007.10.008](https://doi.org/10.1016/j.optcom.2007.10.008).
- 358 [33] M. Schatzl, F. Hackl, M. Glaser, P. Rauter, M. Brehm, L. Spindlberger, A. Simbula, M. Galli,
359 T. Fromherz and F. Schäffler, *Enhanced telecom emission from single group-iv quantum dots*
360 *by precise cmos-compatible positioning in photonic crystal cavities*, *ACS Photonics* **4**(3),
361 665 (2017), doi:[10.1021/acsphotonics.6b01045](https://doi.org/10.1021/acsphotonics.6b01045).
- 362 [34] H.-J. Joo, Y. Kim, D. Burt, Y. Jung, L. Zhang, M. Chen, S. J. Parluhutan, D.-H.
363 Kang, C. Lee, S. Assali, Z. Ikonic, O. Moutanabbir *et al.*, *1D photonic crystal direct*
364 *bandgap GeSn-on-insulator laser*, *Applied Physics Letters* **119**(20), 201101 (2021),
365 doi:[10.1063/5.0066935](https://doi.org/10.1063/5.0066935).
- 366 [35] C. V. Falub, H. Von Känel, F. Isa, R. Bergamaschini, A. Marzegalli, D. Chrastina,
367 G. Isella, E. Müller, P. Niedermann and L. Miglio, *Scaling hetero-epitaxy from*
368 *layers to three-dimensional crystals*, *Science* (80-.). **335**(6074), 1330 (2012),
369 doi:[10.1126/science.1217666](https://doi.org/10.1126/science.1217666).

- 370 [36] J. Pedrini, P. Biagioni, A. Ballabio, A. Barzaghi, M. Bonzi, E. Bonera, G. Isella and
371 F. Pezzoli, *Broadband control of the optical properties of semiconductors through*
372 *site-controlled self-assembly of microcrystals*, *Optics Express* **28**(17), 24981 (2020),
373 doi:[10.1364/oe.398098](https://doi.org/10.1364/oe.398098).
- 374 [37] J. Pedrini, A. Barzaghi, J. Valente, D. J. Paul, G. Isella and F. Pezzoli, *Photonic Band*
375 *Gap and Light Routing in Self-Assembled Lattices of Epitaxial Ge -on- Si Microstructures*,
376 *Physical Review Applied* **16**(6), 1 (2021), doi:[10.1103/PhysRevApplied.16.064024](https://doi.org/10.1103/PhysRevApplied.16.064024).
- 377 [38] V. Falcone, A. Ballabio, A. Barzaghi, C. Zucchetti, L. Anzi, F. Bottegoni, J. Frige-
378 rioro, R. Sordan, P. Biagioni and G. Isella, *Graphene/Ge microcrystal pho-*
379 *todetectors with enhanced infrared responsivity*, *APL Photonics* **7**(4) (2022),
380 doi:[10.1063/5.0082421](https://doi.org/10.1063/5.0082421), 046106, [https://pubs.aip.org/aip/app/article-pdf/doi/10.](https://pubs.aip.org/aip/app/article-pdf/doi/10.1063/5.0082421/16492443/046106_1_online.pdf)
381 [1063/5.0082421/16492443/046106_1_online.pdf](https://pubs.aip.org/aip/app/article-pdf/doi/10.1063/5.0082421/16492443/046106_1_online.pdf).
- 382 [39] Y. H. He, Y. F. Gao, H. Z. Lin, M. C. Jin, Y. He and X. F. Qi, *Topological edge and corner states*
383 *based on the transformation and combination of photonic crystals with square lattice*, *Optics*
384 *Communications* **512**(January), 128038 (2022), doi:[10.1016/j.optcom.2022.128038](https://doi.org/10.1016/j.optcom.2022.128038).
- 385 [40] B. Y. Xie, G. X. Su, H. F. Wang, H. Su, X. P. Shen, P. Zhan, M. H. Lu, Z. L. Wang
386 and Y. F. Chen, *Visualization of Higher-Order Topological Insulating Phases in Two-*
387 *Dimensional Dielectric Photonic Crystals*, *Physical Review Letters* **122**(23), 233903
388 (2019), doi:[10.1103/PhysRevLett.122.233903](https://doi.org/10.1103/PhysRevLett.122.233903).
- 389 [41] X. D. Chen, W. M. Deng, F. L. Shi, F. L. Zhao, M. Chen and J. W. Dong, *Direct Observation of*
390 *Corner States in Second-Order Topological Photonic Crystal Slabs*, *Physical Review Letters*
391 **122**(23), 233902 (2019), doi:[10.1103/PhysRevLett.122.233902](https://doi.org/10.1103/PhysRevLett.122.233902), [1812.08326](https://arxiv.org/abs/1812.08326).
- 392 [42] K. H. Kim and K. K. Om, *Multiband Photonic Topological Valley-Hall Edge Modes and*
393 *Second-Order Corner States in Square Lattices*, *Advanced Optical Materials* **9**(8), 1 (2021),
394 doi:[10.1002/adom.202001865](https://doi.org/10.1002/adom.202001865).
- 395 [43] M. Makwana, R. Craster and S. Guenneau, *Topological beam-splitting in photonic crystals*,
396 *Optics Express* **27**(11), 16088 (2019).
- 397 [44] F. Isa, M. Salvalaglio, Y. A. R. Dasilva, M. Meduña, M. Barget, A. Jung, T. Kreiliger,
398 G. Isella, R. Erni, F. Pezzoli, E. Bonera, P. Niedermann *et al.*, *Highly Mismatched,*
399 *Dislocation-Free SiGe/Si Heterostructures*, *Advanced Materials* **28**(5), 884 (2016),
400 doi:[10.1002/adma.201504029](https://doi.org/10.1002/adma.201504029).
- 401 [45] F. Montalenti, F. Rovaris, R. Bergamaschini, L. Miglio, M. Salvalaglio, G. Isella, F. Isa
402 and H. V. Känel, *Dislocation-Free SiGe/Si Heterostructures*, *Crystals* **8**(257), 1 (2018),
403 doi:[10.3390/cryst8060257](https://doi.org/10.3390/cryst8060257).
- 404 [46] R. Bergamaschini, F. Isa, C. V. Falub, P. Niedermann, E. Müller, G. Isella, H. Von Känel
405 and L. Miglio, *Self-aligned Ge and SiGe three-dimensional epitaxy on dense Si pillar arrays*,
406 *Surface Science Reports* **68**(3-4), 390 (2013), doi:[10.1016/j.surfrep.2013.10.002](https://doi.org/10.1016/j.surfrep.2013.10.002).
- 407 [47] F. Pezzoli, F. Isa, G. Isella, C. V. Falub, T. Kreiliger, M. Salvalaglio, R. Bergamaschini,
408 E. Grilli, M. Guzzi, H. Von Känel and L. Miglio, *Ge Crystals on Si Show Their Light*,
409 *Physical Review Applied* **1**(4), 1 (2014), doi:[10.1103/PhysRevApplied.1.044005](https://doi.org/10.1103/PhysRevApplied.1.044005).
- 410 [48] F. Pezzoli, A. Giorgioni, K. Gallacher, F. Isa, P. Biagioni, R. W. Millar, E. Gatti, E. Grilli,
411 E. Bonera, G. Isella, D. J. Paul and L. Miglio, *Disentangling nonradiative recombination*
412 *processes in Ge micro-crystals on Si substrates*, *Applied Physics Letters* **108**(26) (2016),
413 doi:[10.1063/1.4955020](https://doi.org/10.1063/1.4955020), [1603.08700](https://arxiv.org/abs/1603.08700).

- 414 [49] T. Amotchkina, M. Trubetskov, D. Hahner and V. Pervak, *Characterization of e-beam evap-*
415 *orated ge, ybf3, zns, and laf3 thin films for laser-oriented coatings*, Applied Optics **59**(5),
416 A40 (2020), doi:[10.1364/AO.59.000A40](https://doi.org/10.1364/AO.59.000A40).
- 417 [50] *Comsol multiphysics® v. 5.6.*, www.comsol.com. comsol ab, stockholm, sweden.
- 418 [51] J. D. Joannopoulos, *Photonic Crystals: Molding the Flow of Light*, Princeton University
419 Press, 2 edn., ISBN 978-0691124568 (2008).
- 420 [52] G. Dehlinger, L. Diehl, U. Gennser, H. Sigg, J. Faist, K. Ensslin, D. Grützmacher and
421 E. Müller, *Intersubband electroluminescence from silicon-based quantum cascade structures*,
422 Science **290**(5500), 2277 (2000), doi:[10.1126/science.290.5500.2277](https://doi.org/10.1126/science.290.5500.2277).
- 423 [53] D. J. Paul, *The progress towards terahertz quantum cascade lasers on silicon substrates*,
424 Laser and Photonics Reviews **4**(5), 610 (2010), doi:[10.1002/lpor.200910038](https://doi.org/10.1002/lpor.200910038).
- 425 [54] W. P. Su, J. R. Schrieffer and A. J. Heeger, *Solitons in polyacetylene*, Physical Review
426 Letters **42**(25), 1698 (1979), doi:[10.1103/PhysRevLett.42.1698](https://doi.org/10.1103/PhysRevLett.42.1698).
- 427 [55] F. Liu and K. Wakabayashi, *Novel Topological Phase with a Zero Berry Curvature*, Physical
428 Review Letters **118**(7), 1 (2017), doi:[10.1103/PhysRevLett.118.076803](https://doi.org/10.1103/PhysRevLett.118.076803), [1711.08712](https://doi.org/10.1103/PhysRevLett.118.076803).
- 429 [56] J. Zak, *Berry's phase for energy bands in solids*, Phys. Rev. Lett. **62**, 2747 (1989),
430 doi:[10.1103/PhysRevLett.62.2747](https://doi.org/10.1103/PhysRevLett.62.2747).
- 431 [57] W. A. Benalcazar, T. Li and T. L. Hughes, *Quantization of fractional corner charge in C_n -*
432 *symmetric higher-order topological crystalline insulators*, Phys. Rev. B **99**, 245151 (2019),
433 doi:[10.1103/PhysRevB.99.245151](https://doi.org/10.1103/PhysRevB.99.245151).
- 434 [58] Y. Gong, S. Wong, A. J. Bennett, D. L. Huffaker and S. S. Oh, *Topological in-*
435 *insulator laser using valley-hall photonic crystals*, ACS Photonics **7**(8), 2089 (2020),
436 doi:[10.1021/acsp Photonics.0c00521](https://doi.org/10.1021/acsp Photonics.0c00521).
- 437 [59] M. I. Shalaev, W. Walasik, A. Tsukernik, Y. Xu and N. M. Litchinitser, *Robust topologi-*
438 *cally protected transport in photonic crystals at telecommunication wavelengths*, Nature
439 Nanotechnology **14**(1), 31 (2019), doi:[10.1038/s41565-018-0297-6](https://doi.org/10.1038/s41565-018-0297-6).
- 440 [60] A. B. Khanikaev and G. Shvets, *Two-dimensional topological photonics*, Nature Photonics
441 **11**(12), 763 (2017), doi:[10.1038/s41566-017-0048-5](https://doi.org/10.1038/s41566-017-0048-5).
- 442 [61] B. Y. Xie, H. F. Wang, H. X. Wang, X. Y. Zhu, J. H. Jiang, M. H. Lu and Y. F. Chen,
443 *Second-order photonic topological insulator with corner states*, Physical Review B **98**(20),
444 1 (2018), doi:[10.1103/PhysRevB.98.205147](https://doi.org/10.1103/PhysRevB.98.205147), [1805.07555](https://arxiv.org/abs/1805.07555).
- 445 [62] L. Zhang, Y. Yang, Z. K. Lin, P. Qin, Q. Chen, F. Gao, E. Li, J. H. Jiang, B. Zhang and
446 H. Chen, *Higher-Order Topological States in Surface-Wave Photonic Crystals*, Advanced
447 Science **7**(6) (2020), doi:[10.1002/advs.201902724](https://doi.org/10.1002/advs.201902724).
- 448 [63] J. Bravo-Abad, A. Rodriguez, P. Bermel, S. G. Johnson, J. D. Joannopoulos and M. Sol-
449 jačić, *Enhanced nonlinear optics in photonic-crystal microcavities*, Optics Express **15**(24),
450 16161 (2007), doi:[10.1364/OE.15.016161](https://doi.org/10.1364/OE.15.016161).
- 451 [64] F. Gao, H. Xue, Z. Yang, K. Lai, Y. Yu, X. Lin, Y. Chong, G. Shvets and B. Zhang, *Topolog-*
452 *ically protected refraction of robust kink states in valley photonic crystals*, Nature Physics
453 **14**(2), 140 (2018), doi:[10.1038/nphys4304](https://doi.org/10.1038/nphys4304), [1706.04731](https://arxiv.org/abs/1706.04731).